Materials Research. 2019; 22(6): e20190434
DOI: https//doi.org/10.1590/1980-5373-MR-2019-0434

The Effect of Electropulsing Treatment on Properties of Pre-compressed AZ31 Magnesium Alloy

Xing-xiao Zhu*[a,b], *Xue-wen Zhang*[a,b], *Li-fei Wang*[a,b,c], *Zhi-qing Chen*[a,b], *Xiao-qing Cao*[a,b]

[a] *Shanxi Key Laboratory of Advanced Magnesium-Based Materials, Taiyuan 030024, China*
[b] *College of Materials Science and Engineering, Taiyuan University of Technology, Taiyuan 030024, China*
[c] *School of Materials Science and Engineering, Seoul National University, Seoul, 08826, Korea*

Received: July 19, 2019; Revised: October 28, 2019; Accepted: December 19, 2019

The effect of electropulsing treatment (EPT) on quasi-static compression behavior and anisotropy of AZ31 Mg alloy were investigated based on quasi-static compression test. The results show that the orientation of the sample has a significant effect on the deformation mechanism of metal and this mechanism can be changed by pre-deformation and EPT. However, the strain rate sensitivity of the material is not affected by pre-deformation. Compared with the as-received plates, the anisotropy of AZ31 Mg alloy increased in ND-RD plane after pre-compression along the transverse direction, the ΔYS of specimens increased from 87 MPa to 98 MPa. After EPT, the anisotropy of AZ31 Mg alloy gradually decreased with the change of EPT temperature and EPT time, the ΔYS of the sample reached 14.2 MPa when EPT conducted at 200 ℃ for 15 min, which decreased 72.8 MPa compared with the as-received plates.

Keywords: *AZ31 Mg alloy, Mechanical properties, Pre-compression, Anisotropy, Deformation mechanism.*

1. Introduction

As a lightweight engineering structural material, magnesium alloy has been widely used in automotive and other fields in recent years owing to their high specific strength, excellent damping property and so on [1-2]. However, due to the hexagonal close-packed (HCP) structure of magnesium alloy, there are only two slipping systems at room temperature (RT), which results in poor plasticity of magnesium alloy and limits its application [3-4]. It is well known that twinning can coordinate the plasticity of magnesium alloy [5-6], and it can be twinned by pre-deformation [7-10]. The various of twins can be produced by different methods. There are three types of twins commonly found in magnesium alloys such as {10-12} extension twins, {10-11} compression twins, and {10-13} compression twins. In general, {10-12} extension twins generated when the crystal grains are subjected to stretch along the c-axis direction while {10-11} compression twins are generated when compression is applied along the c-axis direction. Besides, different types of twins have different sensitivity to recovery and recrystallization caused by conventional heat treatment (CHT). Zeng et al. [11] found that {10-11} compression twins are easier to nucleate and recrystallize in CHT compared with {10-12} extension twins. As a mature heat treatment method, CHT is widely used among researchers all over the world. However, CHT has lower heating efficiency and higher energy consumption. In order to reduce energy consumption and improve heating efficiency, numerous studies have been focused on developing a new heat treatment method for alloys [12-20]. In recent years, electropulsing treatment (EPT) has been suggested to be an effective method to control the microstructure of metal materials. Saber et al. [12] found that pulse electrodeposition exhibited marked advantages in the control of deposit grain size, surface morphology, and preferred orientations. Lin et al. [13] found that the pulse current can decrease the dynamic recrystallization (DRX) temperature of AZ31 magnesium alloy. The CHT produced DRX at 200 ℃, but EPT occurred at 150 ℃. The mechanism of EPT includes thermal and non-thermal effects [14-17]. Although people have done a lot of work to study the influence of pulse current on metal structure and properties, but less attention has been paid on the effect of EPT on the anisotropy of magnesium alloy.

In this study, the EPT was conducted on the specimens pre-compressed along the transverse direction (TD) to explore the effect of electropulsing treatment on the properties of pre-compressed AZ31 magnesium alloy. Besides, the cylindrical specimens in both directions of normal direction (ND) and rolling direction (RD) were prepared for compression tests to analyze the anisotropy changes.

2. Materials and Experimental Procedure

A commercial hot-rolled plate of AZ31 magnesium alloy with a thickness of 5 mm was used in this study. The

*email: caoxiaoqing@tyut.edu.cn

AZ31 plate was cut into cuboid specimens with a length of 50 mm and a width of 10 mm by a wire cutting machine (DK7735). The cuboid specimens were compressed with a strain of 4 % along transverse direction by a Hydraulic Press machine (ZLC3000) at a speed of 3 mm/min. The compressed cuboid specimens were subjected to EPT, subsequently. The EPT was carried out using a power supply (CTNP-12/2000-6000 FN) and electropulsing parameters, including the heating temperature and EPT processing time, were listed in Table 1. The duty ratio of the EPT is 50 %, and the frequency is 1000 Hz. The pre-compressed specimens are heated to 100 ℃, 150 ℃ and 200 ℃ by EPT, then maintained for 5 min, 10 min, 15 min, respectively. The temperature of the samples was measured by a thermocouple (TM6902D) during the test. Furthermore, an infrared thermal imager (UTI160G) was used to correct the error in the measurement. The metallographic analysis was performed by optical microscopy (OM; Leica DM2700M).

The variation of quasi-static compression properties of magnesium alloys was investigated by comparing the compression properties of EPT specimens and non-EPT specimens. The compression tests were performed over a strain rate ranging from approximately 10^{-4} s^{-1} to 10^{-2} s^{-1} by a universal testing machine (DNS200). All quasi-static compression tests were conducted on cylindrical specimens with 5 mm in diameter and 4 mm in height. The schematic diagram of compression specimens was shown in Figure 1. Three specimens were used for each group of experiments for accuracy. Finally, the quasi-static compression parameters, including as-received specimens and TD pre-compression specimens, were listed in Table 2.

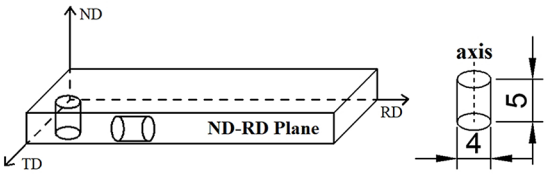

Figure 1. Schematic diagram of the compression specimens used in deformation tests.

Table 2. Compression test conditions for AZ31 specimens.

	Cutting methods	Initial strain rate	Type
as-received	axis//ND	10^{-4} s^{-1}	as-ND
	axis//ND	10^{-3} s^{-1}	as-ND
	axis//ND	10^{-2} s^{-1}	as-ND
	axis//RD	10^{-4} s^{-1}	as-RD
	axis//RD	10^{-3} s^{-1}	as-RD
	axis//RD	10^{-2} s^{-1}	as-RD
TD pre-compression	axis//ND	10^{-4} s^{-1}	T-ND
	axis//ND	10^{-3} s^{-1}	T-ND
	axis//ND	10^{-2} s^{-1}	T-ND
	axis//RD	10^{-4} s^{-1}	T-RD
	axis//RD	10^{-3} s^{-1}	T-RD
	axis//RD	10^{-2} s^{-1}	T-RD

Table 1. Compression test conditions for TD pre-compression EPT specimens.

Cutting methods	Temperature	Time	Initial strain rate	Type
axis//ND	100 ℃	5min	10^{-3} s^{-1}	100 ℃ T-ND
axis//ND	150 ℃	5min	10^{-3} s^{-1}	150 ℃ T-ND
axis//ND	200 ℃	5min	10^{-3} s^{-1}	200 ℃ T-ND
axis//RD	100 ℃	5min	10^{-3} s^{-1}	100 ℃ T-RD
axis//RD	150 ℃	5min	10^{-3} s^{-1}	150 ℃ T-RD
axis//RD	200 ℃	5min	10^{-3} s^{-1}	200 ℃ T-RD
axis//ND	100 ℃	10min	10^{-3} s^{-1}	100 ℃ T-ND
axis//ND	150 ℃	10min	10^{-3} s^{-1}	150 ℃ T-ND
axis//ND	200 ℃	10min	10^{-3} s^{-1}	200 ℃ T-ND
axis//RD	100 ℃	10min	10^{-3} s^{-1}	100 ℃ T-RD
axis//RD	150 ℃	10min	10^{-3} s^{-1}	150 ℃ T-RD
axis//RD	200 ℃	10min	10^{-3} s^{-1}	200 ℃ T-RD
axis//ND	100 ℃	15min	10^{-3} s^{-1}	100 ℃ T-ND
axis//ND	150 ℃	15min	10^{-3} s^{-1}	150 ℃ T-ND
axis//ND	200 ℃	15min	10^{-3} s^{-1}	200 ℃ T-ND
axis//RD	100 ℃	15min	10^{-3} s^{-1}	100 ℃ T-RD
axis//RD	150 ℃	15min	10^{-3} s^{-1}	150 ℃ T-RD
axis//RD	200 ℃	15min	10^{-3} s^{-1}	200 ℃ T-RD

3. Result and Discussion

3.1 Microstructures evolution

The microstructure of the as-received sample and the T-ND sample were shown in Figure 2. It can be seen that the average grain size of the as-received sample is 15.1 μm and the microstructure is composed of many fine equiaxed grains with large grains around them, as shown in Figure 2a. When the plate is subjected to TD pre-compression, a large number of twins are generated. As a mechanism for coordinating plastic deformation, the grain orientation can be effectively adjusted by twins. In general, when the grains are stretched along the c-axis direction or compressed perpendicular to the c-axis direction, {10-12} extension twins are generated, and the base plane of the twins is rotated 86° along <1-210> direction 18. Figure 3 shows the microstructure of specimens after the EPT. It can be seen that there is no significant change in the grain size of the specimens and the proportion of the twins when EPT temperature is below 150 ℃ and the EPT time is less than 15 min. The grain size of sample increased and the proportion of twins decreased but did not disappear completely when EPT conducted at 150 ℃ for 15 min. When the temperature of EPT increased to 200 ℃, the number of twins gradually decreased and the size of grains gradually increased with increasing the processing time of EPT. When the sample was maintained at 200 ℃ for 10 minutes, the twins completely disappeared and the grains grew significantly with an average grain size was 16.4 μm. Moreover, the grains continued to grow and the average grain size was 33.2 μm as the EPT time was increased to 15 minutes. Compared with the CHT, the recovery and recrystallization behaviors of the sample is more efficiently under the EPT. Heating in a short period at 200 ℃ for 10 min can result in all the twins disappear in the alloy. It can be inferred that the nucleation rate and atomic diffusion were increased significantly owing to the coupling effects of the thermal and athermal effects of EPT, which promotes the grains to nucleate and grow at the twins' boundary and lead to the disappearance of the twins. Jiang et al. [19] also found that EPT can accelerate the recrystallization process of the cold-rolled Mg-9Al-1Zn alloy at lower temperatures and induce changes in microstructure to weaken the base texture.

3.2 The compression behavior of the as-received plate

The compression true stress-strain curves at initial strain rate of 10^{-2} s^{-1}; 10^{-3} s^{-1}; 10^{-4} s^{-1} for as-ND and as-RD were shown in Figure 4a. The engineering stress and engineering strain can be obtained as follows.

$$\sigma_e = \frac{P}{A_0} \tag{1}$$

$$\varepsilon_e = \frac{\delta}{L_o} \tag{2}$$

where σ_e is the engineering stress (MPa), ε_e the engineering strain, P the load force (N), δ the displacement of specimen (mm), A_0 the cross sectional area (mm^2), L_0 the height of specimen (mm). The true stress σ_t and true strain ε_t need to be converted from engineering stress and strain using the following equations:

$$\sigma_t = -\ln(1-\varepsilon_e) \tag{3}$$

$$\varepsilon_t = \sigma_e(1-\varepsilon_e) \tag{4}$$

Similar to the experimental results of Yang [20], the samples compressed along different directions exhibited different deformation behavior at RT. Irrespective of the strain rates, the curves of as-ND and as-RD showed yielding at about 150 MPa and 85 MPa followed by work hardening, respectively. For the true stress-strain curves of as-ND specimens, the curves show the conventional work hardening phenomenon, and the work hardening rate decreased with the increase of strain, as shown in Figure 4b. For the true stress-strain curves of as-RD specimens, regardless of the strain rates, there is an inflexion point when the strain is about 11%, and

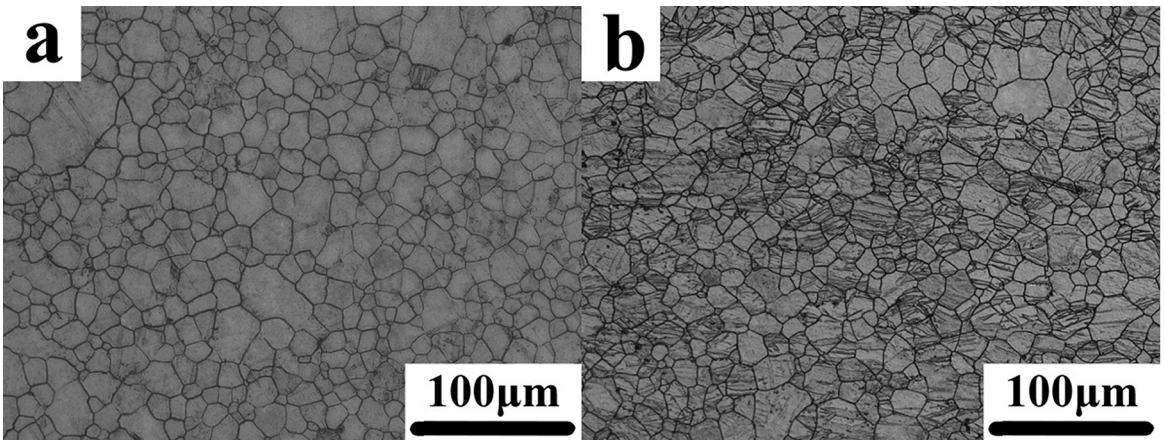

Figure 2. OM micrographs of specimens. (a) as-ND; (b) T-ND

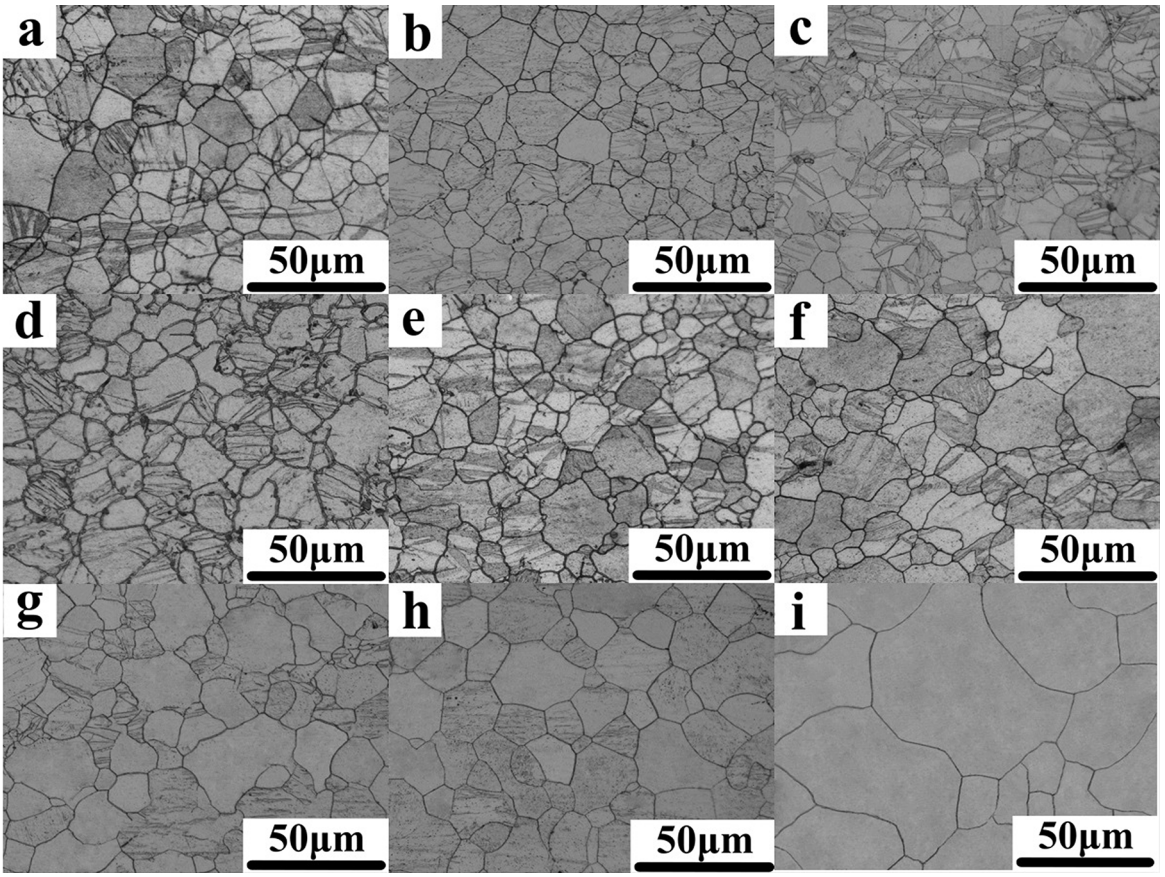

Figure 3. OM micrographs of specimens after the EPT.
(a)100 °C 5min T-ND; (b)100 °C 10min T-ND;(c)100 °C 15min T-ND
(d)150 °C 5min T-ND; (e)150 °C 10min T-ND;(f)150 °C 15min T-ND
(g)200 °C 5min T-ND; (h)200 °C 10min T-ND;(i)200 °C 15min T-ND

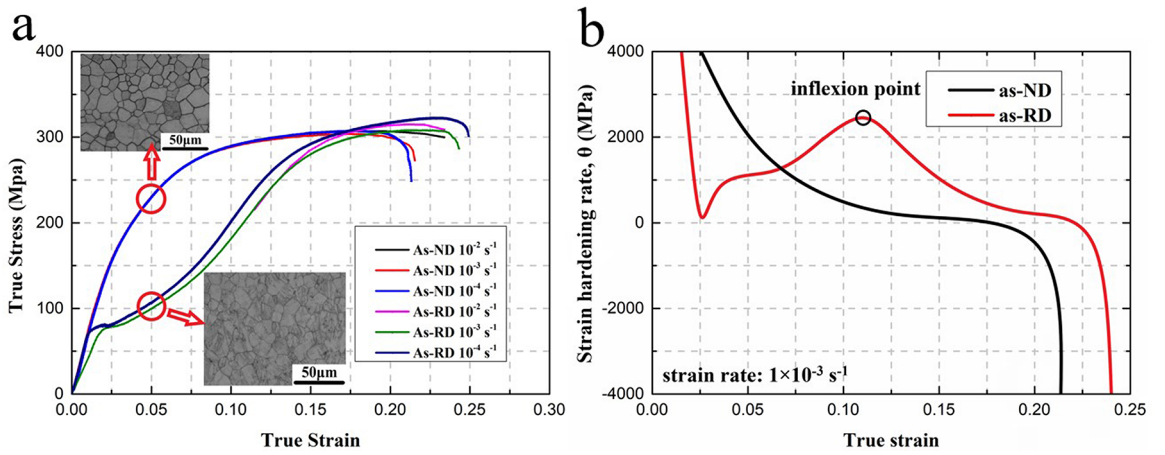

Figure 4. Specimens compressed at a strain rate range of 10^{-4} s^{-1}~10^{-2} s^{-1} (a) True stress-strain curves; (b) Strain hardening curves.

the curves show the conventional work hardening behavior after the inflection point. Before that, the strain hardening rate was increased with the increase of strain.

The curves' shape of as-ND and as-RD are significantly different, which indicates that there are significant differences in the deformation mechanism between two samples. When the as-ND sample is compressed along the c-axis at RT, {10-11} compression twins will produce, but the {10-11} compression twins are not easily formed at RT and it requires a large amount of deformation [21-24]. From the OM micrographs in Figure 4a, it can be seen that no twins existed in grains when the strain of as-ND reaches 5%.

Therefore, {10-11} compression twins did not formed in as -ND samples during the deformation process. It indicates that the dominant deformation mechanism of as-ND during compression is crystallographic slip. The concaved down shape of As-ND true stress-strain curves should be attributed to the crystallographic slip which leads to the rapid initial work hardening. When the grains are pressed along the direction perpendicular to the c-axis, the {10-12} extension twins will preferentially generate and coordinate the deformation of the metal due to the critical resolved shear stress (CRSS) of the {10-12} extension twins is smaller than that of slipping, as shown in Figure 4a. Therefore, the dominant deformation mechanism of as-RD during compression is twinning, and the concaved up shape of as-RD true stress-strain curves can be explained by that the dominant deformation of twinning leads to little strain hardening at the early deformation stage, only when the twinning capacity is exhausted, strong work hardening due to slip and slip-twinning interaction is achieved [25].

At the beginning of the curves of as-ND and as-RD, work hardening behavior occurs on magnesium alloy, it can be seen that the flow stress increased gradually with the increase of strain, but the flow stress does not change significantly among three strain rates. It indicates that the flow stress of AZ31 magnesium alloy is not sensitive to the quasi-static strain rate.

3.3 The compression behavior after TD pre-deformation

There is no doubt that the texture plays an important role in plastic deformation of metals with hexagonal crystal structure. Samples with different initial texture exhibited a different deformation behavior, as shown in Figure 5a and Figure 5b.

When the cuboid samples is pre-compressed along the transverse direction, {10-12} tension twins are generated. From the shape of the curves in Figure 5a, it can be seen that the deformation mechanism has changed significantly between T-ND and as-ND, the dominant deformation mechanism of as-ND is crystallographic slip, but twinning for the T-ND. From the shape of curves in Figure 5b we can consider that the deformation mechanisms of T-RD and as-RD are similar. This is because that the quasi-static compression test makes the c-axes of grains subjected to indirectly tension and generated {10-12} extension twins, as shown in Table 3, the deformation mechanisms of T-RD and as-RD are twinning.

Table 3. The relative orientation between basal planes and c-axis with the loading direction.

Compression	ND	RD
	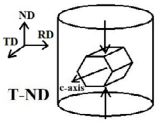	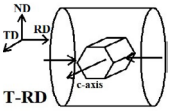
	Basal planes parallel to the compression direction.	Basal planes parallel to the compression direction.
	c-axis subject to indirectly tension.	c-axis subject to indirectly tension.

Besides, comparing the pre-deformed samples and the as-received samples at three strain rates, we found that the strain rate sensitivity does not change after metal pre-deformation. The flow stress of AZ31 magnesium alloy is not sensitive to the quasi-static strain rate.

3.4 The compression behavior after EPT

Typical true stress-strain curves determined at various conditions are plotted in Figure 6. It can be seen that there is no significant change in the deformation mechanism of specimens when EPT temperature is below 200 °C and EPT time is less than 10 min.

When the EPT temperature is lower than 150 °C and the EPT time is less than 15 min, we can find from Figure 3a-e that the morphology of the grains is still dominated

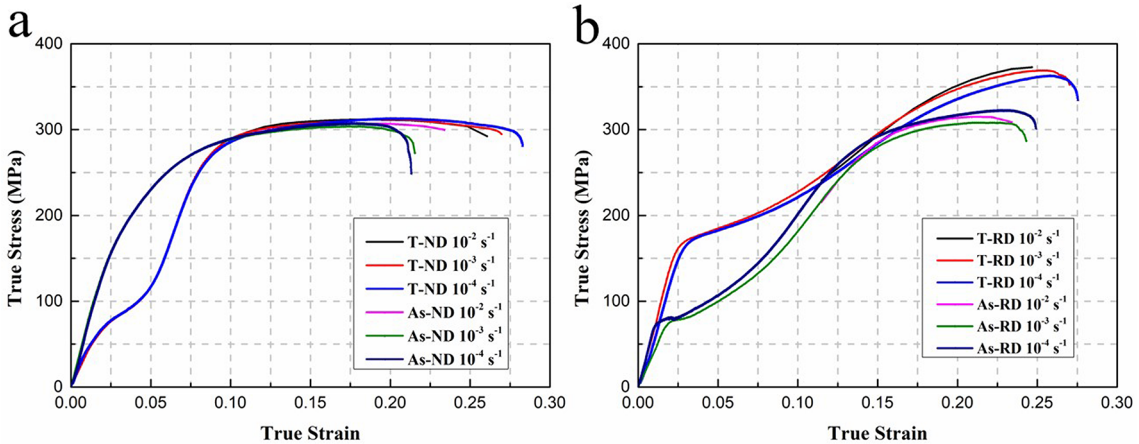

Figure 5. True stress–strain curves of specimens obtained from quasi-static compression tests. (a) axis//ND (b) axis//RD

by large-area twins. On the other hand, The shape of those of the curves those of the T-ND and T-RD samples after EPT is similar to the T-ND and T-RD samples before EPT, as shown in Figures 6a-b. This indicated that the dominant deformation mechanism of "100 ℃ T-ND" and "100 ℃ T-RD" samples are not changed compared with the T-ND sample, the dominant deformation mechanism is still twinning. When EPT 15 min at 150 ℃, most of grains nucleated at twins' boundary and grew into new grains, from Figure 3f we can see that the proportion of twins was reduced greatly. Besides, we can infer from the shape of the true stress-strain curves of the sample in Figure 6c that the deformation mechanism of the sample begins to change, but it is still dominated by twinning.

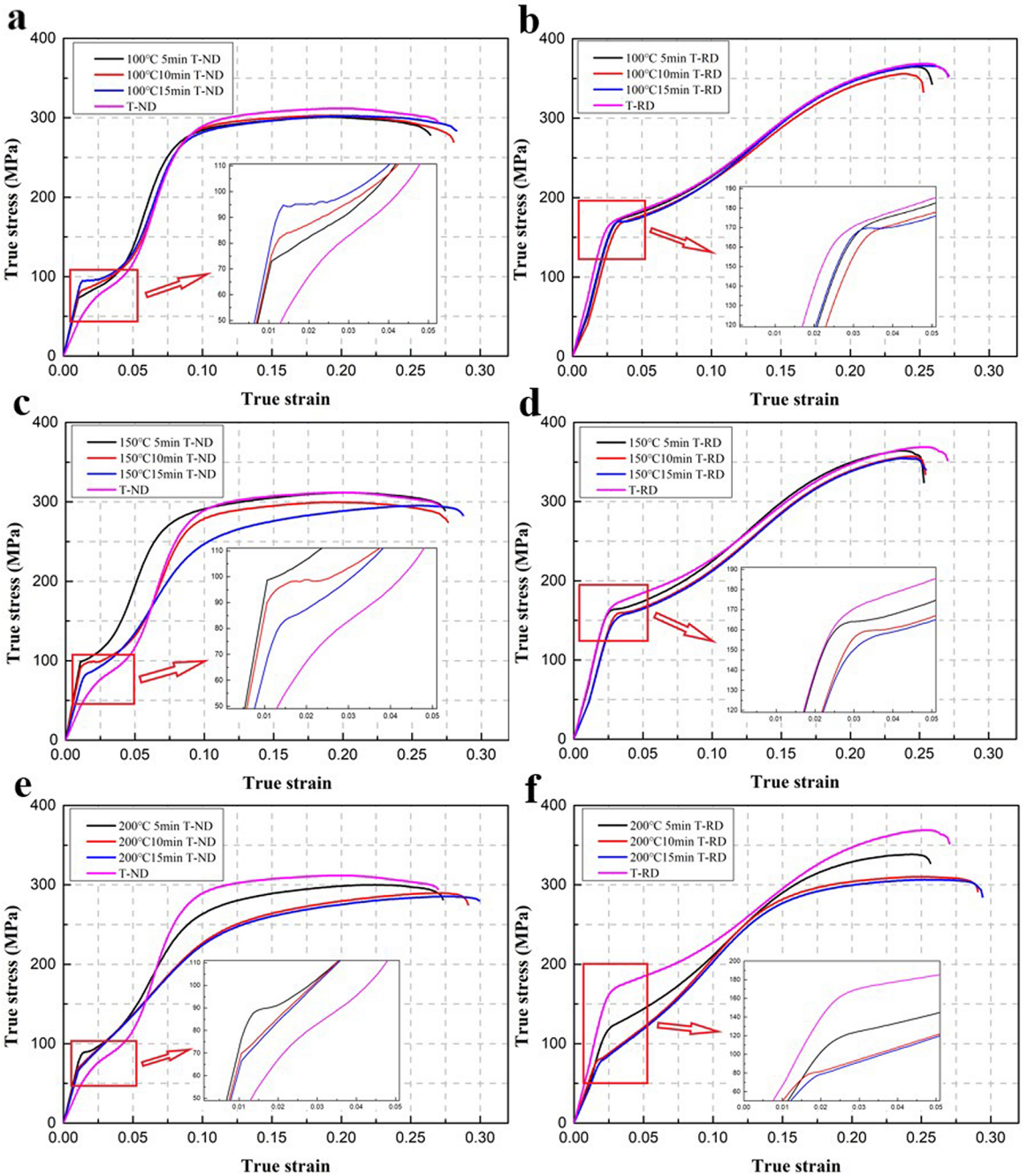

Figure 6. True stress–strain curves of specimens after EPT.
(a) EPT 100 ℃ T-ND; (b) EPT 100 ℃ T-RD; (c) EPT 150 ℃ T-ND
(d) EPT 150 ℃ T-RD; (e) EPT 200 ℃ T-ND; (f) EPT 200 ℃ T-RD

When EPT 10 min and 15 min at 200 ℃, we can easily find that the twins have completely disappeared from the OM micrograph in Figure 3h-i, the microstructure is consisted of uniform large grains. On the other hand, the shape of the true stress-strain curves of 200 ℃ T-ND and 200 ℃ T-RD samples starts to change from concave up to concave down, and the shape of the curve is similar to As-ND sample, which means that the deformation mechanism of the sample begins to change from twinning to crystallographic slip.

3.5 Anisotropy analysis before and after EPT

In order to analyze the effect of EPT on the anisotropy of magnesium alloys, we have compiled the yield strength (YS) of the specimens into Table 4 and the results of the difference in YS between ND and RD (ΔYS) of different specimens were shown in Figure 7. The results show that the quasi-static compression behavior of AZ31 magnesium alloy exhibits anisotropy in ND-RD plane.

From the data in Table 4 we can see that the yield strength of as-ND and as-RD were 153.6 MPa and 66.6 MPa, respectively. Compared with the ΔYS of 87 MPa of the as-received plates, the ΔYS of the plate in the ND-RD plane increased from 87 MPa to 98 MPa after TD pre-compression. This is because the broken and fibrillated grains caused by the pre-compression resulting in the generation of residual stress inside the magnesium alloy. Grains inside the magnesium alloy began to slip and dislocation entanglement occurred, then the work hardening occurred accordingly, which lead to the increase of the YS of "non-EPT T-RD" sample from 66.6 MPa to 158.8 MPa. Besides, due to the c-axis of the grains was indirectly subjected to stretching, the base plane of twins was rotated 86° along <1-210> direction [18], resulting in the generation of the {10-12} extension twinning and the YS of "non-EPT T-ND" sample was reduced from 153.6 MPa to 60.8 MPa.

After EPT, the anisotropy of the magnesium alloy on the ND-RD plane gradually decreased with the increase of the EPT time and temperature. When EPT temperature is reached 200 ℃, the ΔYS of the plate in the ND-RD plane is reduced to about 15 MPa. We can easily find the YS of RD samples decreased with the increase of EPT time and temperature from the data in Table 4. This can be attributed to the great contribution of the EPT. When the EPT was applied to magnesium alloy, due to the recovery and recrystallization of the grains, the dislocation density and residual stress inside the magnesium alloy were greatly reduced, which leads to the weakening of work hardening behavior. On the other hand, although recovery and recrystallization occurred in the "EPT T-ND" sample, the deflection angle of the grains hardly changed. Since the incomplete recrystallization of the metal caused by the EPT, the average grain size of "EPT T-ND" specimens are slightly smaller than the "non-EPT T-ND" sample. Compared with the "non-EPT T-ND" sample, the YS of "EPT T-ND" specimen increased due to the fine-grain strengthening. With the increase of EPT time and temperature, the grains completely recrystallized at 200 ℃ for 15 min, at which the YS of "EPT T-ND" specimen was substantially same as that of "non-EPT T-ND" sample.

In summary, the anisotropy of AZ31 magnesium alloy gradually decreased with the increase of EPT time and temperature. After 10 min and 15 min EPT at 200 °C, the ΔYS of the sample decreased to 14.2 MPa.

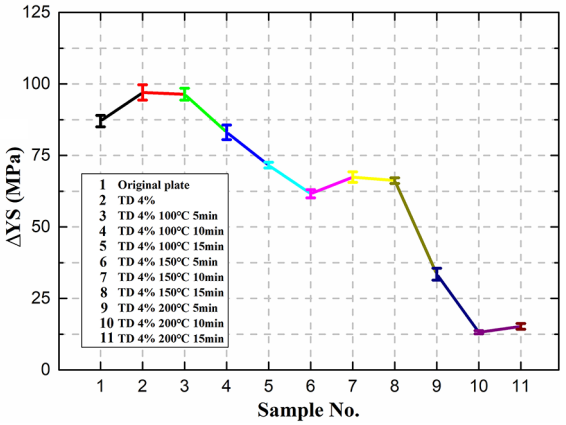

Figure 7. The variation trend of ΔYS under different conditions.

Table 4. Yield strength of the ND and RD specimens at various conditions

Testing Direction	Yield Strength (MPa)										
	as-received		TD pre-compression 4%								
	non-EPT	non-EPT	EPT								
	RT	RT	100 ℃			150 ℃			200 ℃		
	-	-	5min	10min	15min	5min	10min	15min	5min	10min	15min
ND	153.6	60.8	73.1	81.8	94.7	98.7	89.9	81.5	87.7	68.8	66.5
RD	66.6	158.8	170.2	165.2	166.3	159.8	157.2	148.7	121.8	81.3	80.7

4. Conclusion

In the present study, the effect of EPT on quasi-static compression behavior and anisotropy of AZ31 magnesium alloy were investigated. The major results are as follows:

1. Sample compressed along different directions exhibited different deformation mechanisms at RT. The dominant deformation mechanism of as-ND samples are crystallographic slip, but the dominant deformation mechanism of as-RD samples is twinning. After TD pre-deformation, the dominant deformation mechanism of T-ND samples changed from crystallographic slip to twinning, but that of T-RD samples is still dominated by twinning. When the EPT was conducted at 200 ℃ for 10 min and 15 min, the deformation mechanism begins to change from twinning to crystallographic slip.

2. The strain rate sensitivity of the Mg alloy is not affected by pre-deformation. The flow stress of AZ31 Mg alloy is not sensitive to the quasi-static strain rate.

3. Compared with the as-received plates, the anisotropy of AZ31 magnesium alloy increased in the ND-RD plane after pre-compression along the transverse direction, the ΔYS of the samples increased from 87 MPa to 98 MPa. After EPT, the anisotropy of AZ31 magnesium alloy gradually decreased with the change of EPT temperature and EPT time, the ΔYS of the samples reached 14.2 MPa when EPT conducted at 200 ℃ for 15 min, which decreased 72.8 MPa compared with the as-received plates.

5. Acknowledgments

This work was supported by the National Natural Science Foundation of China (grant nos. 51704209 and U1810208); Advanced Programs of Department of Human Resources and Social Security of Shanxi Province for Returned Scholars Scientific (2017014); Technological Innovation Programs of Higher Education Institutions in Shanxi (201802034); The Projects of International Cooperation in Shanxi (201803D421086); and the Research Project Supported by Shanxi Scholarship council of China (grant no. 2015036).

6. References

1. Friedrich HE, Mordike BL. *Magnesium technology*. Berlin: Springer Publishing; 2006.
2. Easton M, Gibson M, Beer A, Barnett M, Davies C, Durandet Y, et al. The application of magnesium alloys to the lightweighting of automotive structures. *Sustainable Automotive Technologies*. 2012;17-23.
3. Abedi H, Zarei-Hanzaki A, Khoddam S. Effect of γ precipitates on the cavitation behavior of wrought AZ31 magnesium alloy. *Materials and Design*. 2011;32(4):2181-2190.
4. Yin DL, Zhang KF, Wang GF, Han WB. Superplasticity and cavitation in AZ31 Mg alloy at elevated temperatures. *Materials Letters*. 2005;59(14-15):1714-1718.
5. Wang L, Cao M, Cheng W, Zhang H, Cao X, Mostaed E. Improved stretch formability of AZ31 magnesium thin sheet by induced {10–12} tension twins. *JOM*. 2018;70(10):2321-2326.
6. Cheng W, Wang L, Zhang H, Cao X. Enhanced stretch formability of AZ31 magnesium alloy thin sheet by pre-crossed twinning lamellas induced static recrystallizations. *Journal of Materials Processing Technology*. 2018;254:302-309.
7. Kang YH, Wang XX, Zhang N, Yan H, Chen RS. Effect of pre-deformation on microstructure and mechanical properties of WE43 magnesium alloy. *Materials Science and Engineering: A*. 2017;689:435-445.
8. Huang G, Han T, Pan F, Zhang H, Li J. Improving low-cycle fatigue properties of rolled AZ31 magnesium alloy by pre-compression deformation. *Materials and Design*. 2014;58:439-444.
9. Sarker D, Friedman J, Chen DL. Influence of pre-deformation and subsequent annealing on strain hardening and anisotropy of AM30 magnesium alloy. *Journal of Alloys and Compounds*. 2014;611:341-350.
10. Sarker D, Chen DL. Dependence of compressive deformation on pre-strain and loading direction in an extruded magnesium alloy: Texture, twinning and de-twinning. *Materials Science and Engineering: A*. 2014;596:134-144.
11. Zeng Z, Xin YC, Wang MY, Liu Q. Influence of twin types on static recrystallization of AZ31 magnesium alloy. *Transactions of Materials and Heat Treatment*. 2012;33(8):33-38.
12. Saber K, Koch CC, Fedkiw PS. Pulse current electrodeposition of nanocrystalline zinc. *Materials Science and Engineering: A*. 2003;341(1-2):174-181.
13. Lin SX, Chu XR, Yue ZM, Gao J. Effect of temperature on the dynamic recrystallization of AZ31 alloy with pulse current. *Acta Metallurgica Sinica (English Letters)*. 2018;31(12):1281-1286.
14. Kim MJ, Lee K, Oh KH, Choi IS, Yu HH, Hong ST, et al. Electric current-induced annealing during uniaxial tension of aluminum alloy. *Scripta Materialia*. 2014;75:58-61.
15. Roh JH, Seo JJ, Hong ST, Kim MJ, Han HN, Roth JT, et al. The mechanical behavior of 5052-H32 aluminum alloys under a pulsed electric current. *International Journal of Plasticity*. 2014;58:84-99.
16. Kim MJ, Lee MG, Hariharan K, Hong ST, Choi IS, Kim D, et al. Electric current–assisted deformation behavior of Al-Mg-Si alloy under uniaxial tension. *International Journal of Plasticity*. 2017;94:148-170.
17. Lee YJ, Sung HM, Jin Y, Lee K, Park CR, Kim GH, et al. Improvement of mechanical property of air plasma sprayed tungsten film using pulsed electric current treatment. *International Journal of Refractory Metals and Hard Materials*. 2016;60:99-103.
18. Barnett MR, Keshavarz Z, Beer AG, Atwell D. Influence of grain size on the compressive deformation of wrought Mg-3Al-1Zn. *Acta Materialia*. 2004;52(17):5093-5103.
19. Jiang Y, Guan L, Tang G, Shek C, Zhang Z. Influence of electropulsing treatment on microstructure and mechanical properties of cold-rolled Mg-9Al-1Zn alloy strip. *Materials Science and Engineering: A*. 2011;528(16-17):5627-5635.

20. Yang YB, Wang FC, Tan CW, Wu YY, Cai HN. Plastic deformation mechanisms of AZ31 magnesium alloy under high strain rate compression. *Transactions of Nonferrous Metals Society of China*. 2008;18(5):1043-1046.

21. Barnett MR. Twinning and the ductility of magnesium alloys: Part I: "Tension" twins. *Materials Science and Engineering: A*. 2007;464(1-2):1-7.

22. Barnett MR. Twinning and the ductility of magnesium alloys: Part II: "Contraction" twins. *Materials Science and Engineering: A*. 2007;464(1-2):8-16.

23. Barnett MR, Nave MD, Bettles CJ. Deformation microstructures and textures of some cold rolled Mg alloys. *Materials Science and Engineering: A.* 2004;386(1-2):205-211.

24. Jiang L, Jonas JJ, Luo AA, Sachdev AK, Godet S. Twinning-induced softening in polycrystalline AM30 Mg alloy at moderate temperatures. *Scripta Materialia*. 2006;54(5):771-775.

25. Mao P, Liu Z, Wang C. Texture effect on high strain rates tension and compression deformation behavior of extruded AM30 alloy. *Materials Science and Engineering: A*. 2012;539:13-21.